An ab Initio Molecular Orbital Study of the Thermal Decomposition of Fluorinated Monosilanes, $SiH_{4-n}F_n$ (n = 0-4)

Edgar W. Ignacio† and H. Bernhard Schlegel*

Department of Chemistry, Wayne State University, Detroit, Michigan 48202 *(Received: June 13, 1991; In Final Form: October 21, 1991)*

The reactants, clusters, transition structures, and products for the various channels for the thermal decomposition of $SiH_{4-n}F_n$ were optimized at the HF/6-31G* level. The electron correlation contributions were calculated at MP4/6-31G* and MP4/6-31G** levels. In the decomposition of SiH_4, $SiH_2 + H_2$ is favored over $SiH_3 + H$. For SiH_3F, the $SiHF + H_2$ channel is preferred over $SiH_2F + H$, $SiH_2 + HF$, and $SiH_3 + F$. In the decomposition of SiH_2F_2, the barrier for the formation of $SiF_2 + H_2$ is slightly lower than those of $SiHF_2 + H$ and $SiHF + HF$, while those of the $SiH_2F + F$ and $SiH_2 + F_2$ channels are considerably higher. For $SiHF_3$, decomposition into $SiF_2 + HF$ is favored with $SiF_3 + H$ lying slightly higher. The other two channels $SiHF_2 + F$ and $SiHF + F_2$ are much higher in energy. In SiF_4, the decomposition into $SiF_3 + F$ is favored over the reaction $SiF_4 \rightarrow SiF_2 + F_2$.

Introduction

The gas-phase stability of small silicon compounds is of considerable interest to the semiconductor industry, especially for processes such as chemical vapor deposition (CVD) of thin films and in etching of silicon surfaces.[1-4] In the chemical vapor deposition of amorphous silicon films, materials such as SiH_4, Si_2H_6, SiF_4, $SiCl_4$, etc. or various mixtures of these are heated to 400-800 °C. Thermal decomposition of the starting materials is the initial step in the deposition. Previous theoretical studies have dealt with the thermal decomposition of SiH_4[1] and Si_2H_6[2] and the heats of formation of SiH_mF_n[3-6] and SiH_mCl_n.[7] The decomposition of $SiH_{4-n}F_n$ is of interest since amorphous silicon films containing small percentages of fluorine have desirable electric properties for photovoltaic devices.[8] In recent experimental work,[9] the rates for unimolecular decomposition of $SiH_{4-n}F_n$ (n = 0, 1, 2) have been determined in the temperature range 1200-2000 K. The present paper outlines a theoretical study of the pathways, transition structures, and barriers for thermal decomposition of SiH_4, SiH_3F, SiH_2F_2, $SiHF_3$, and SiF_4. The following reactions have been considered:

$$SiH_4 \rightarrow SiH_2 + H_2 \quad (1)$$

$$SiH_4 \rightarrow SiH_3 + H \quad (2)$$

$$SiH_3F \rightarrow SiHF + H_2 \quad (3)$$

$$SiH_3F \rightarrow SiH_2 + HF \quad (4)$$

$$SiH_3F \rightarrow SiH_2F + H \quad (5)$$

$$SiH_3F \rightarrow SiH_3 + F \quad (6)$$

$$SiH_2F_2 \rightarrow SiF_2 + H_2 \quad (7)$$

$$SiH_2F_2 \rightarrow SiHF + HF \quad (8)$$

$$SiH_2F_2 \rightarrow SiH_2 + F_2 \quad (9)$$

$$SiH_2F_2 \rightarrow SiHF_2 + H \quad (10)$$

$$SiH_2F_2 \rightarrow SiH_2F + F \quad (11)$$

$$SiHF_3 \rightarrow SiF_2 + HF \quad (12)$$

$$SiHF_3 \rightarrow SiHF + F_2 \quad (13)$$

$$SiHF_3 \rightarrow SiF_3 + H \quad (14)$$

$$SiHF_3 \rightarrow SiHF_2 + F \quad (15)$$

$$SiF_4 \rightarrow SiF_2 + F_2 \quad (16)$$

$$SiF_4 \rightarrow SiF_3 + F \quad (17)$$

These reactions fall into two categories: (a) single bond dissociation (reactions 2, 5, 6, 10, 11, 14, 15, 17) and (b) decomposition into a silylene and a diatomic. The reverse of a single bond dissociation, i.e. simple radical-radical recombination, should have no activation barrier; hence the energy required for these decomposition pathways can be obtained from the heats of formation of the silanes and the silyl radicals. In our previous studies,[3,4] heats of formation were calculated for the various fluorinated silylenes, silyl radicals, and silanes. A reliable set of heats of formation was obtained using the isodesmic reactions

$$(a/n)SiH_n + (b/n)SiF_n \rightarrow SiH_aF_b \; (a + b = n) \quad (18)$$

$$(a/4)SiF_n + [(4 - a)/4]Si \rightarrow SiF_a \; (a = 1, 2, 3) \quad (19)$$

$$SiH_{4-a}F_a + SiH_n \rightarrow SiH_4 + SiF_a \; (a = 1, 2, 3) \quad (20)$$

and combining the theoretical ΔH's calculated at the MP4SDTQ/6-31++G(2d,2p) level or better with the experimental $\Delta H_f°$ for SiH_n and SiF_4. Ho et al.[6] obtained similar results using the bond additivity approach and MP4/6-31G** calculations. The second category of reactions is the reverse of the family of silylene insertions into H_2, HF, and F_2 (reactions 1, 3, 4, 7-9, 12, 13, 16). The insertions of SiH_2, SiHF, and SiF_2 into H_2 were studied in earlier work.[10,11] At the MP4SDQ/6-31G** level, the barrier for insertion is 7.9 kcal/mol for $SiH_2 + H_2$, 30.1 kcal/mol for $SiHF + H_2$, and 61.1 kcal/mol for $SiF_2 + H_2$. More extensive calculations on $SiH_2 + H_2$[1] lead to a barrier of 1.7 kcal/mol, in good agreement with recent experiments.[12] Of the other insertion reactions listed above, only $SiH_2 + HF$ has been studied previously.[13]

In the present paper, transition structures and loose clusters are calculated for $SiHF + HF$, $SiF_2 + HF$, $SiH_2 + F_2$, SiHF +

† Present address: Department of Chemistry, MSU-Iligan Institute of Technology, Iligan City, 9200 Philippines.

(1) Gordon, M. S.; Gano, D. R.; Binkley, J. S.; Frisch, M. J. *J. Am. Chem. Soc.* **1986**, *108*, 2191.
(2) Gordon, M. S.; Truong, T. N.; Bonderson, E. K. *J. Am. Chem. Soc.* **1986**, *108*, 1421.
(3) Schlegel, H. B. *J. Phys. Chem.* **1984**, *88*, 6255.
(4) Ignacio, E. W.; Schlegel, H. B. *J. Chem. Phys.* **1990**, *92*, 5404.
(5) Dixon, D. A. *J. Phys. Chem.* **1988**, *92*, 86.
(6) Ho, P.; Melius, C. F. *J. Phys. Chem.* **1990**, *94*, 5120.
(7) Ho, P.; Coltrin, M. E.; Binkley, J. S.; Melius, C. F. *J. Phys. Chem.* **1985**, *89*, 4647; **1986**, *90*, 3399.
(8) Miller, R. D. In *Silicon Chemistry*; Corey, E. R., Gaspar, P. P., Eds.; Ellis Horwood: Chichester, England, 1988.
(9) Koshi, M.; Kato, S.; Matsui, H. *J. Phys. Chem.* **1991**, *95*, 1223.
(10) Sosa, C.; Schlegel, H. B. *J. Am. Chem. Soc.* **1984**, *106*, 5847.
(11) Schlegel, H. B.; Sosa, C. *J. Phys. Chem.* **1985**, *89*, 537.
(12) Moffat, H. K.; Jensen, K. F.; Carr, R. W. *J. Phys. Chem.* **1991**, *95*, 145 and references therein.
(13) Raghavachari, K.; Chandrasekhar, J.; Gordon, M. S.; Dykema, K. *J. Am. Chem. Soc.* **1984**, *106*, 5853.

0022-3654/92/2096-1620$03.00/0

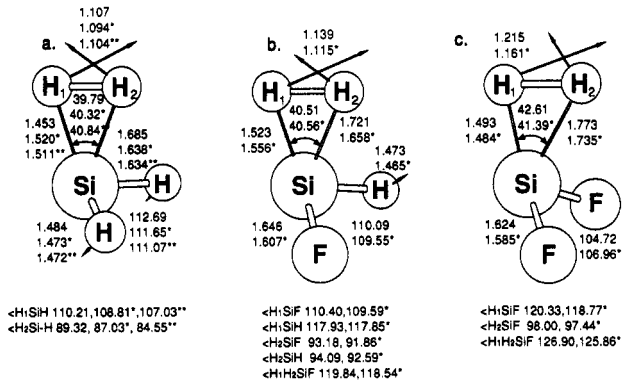

Figure 1. Transition structures for SiH_2, SiHF, and SiF_2 insertion into H_2: no superscript, HF/3-21G optimized; asterisk, HF/6-31G* optimized; double asterisk, MP2/6-31G** optimized. Arrows indicate the HF/6-31G* transition vectors.

F_2, and $SiF_2 + F_2$. These results are combined with previously computed barrier heights for silylene insertions and calculated heats of formation of SiH_nF_m ($n + m = 2, 3, 4$) to estimate the energetics of the various pathways for thermal decomposition of fluorine-substituted silanes.

Computational Method

Ab initio MO calculations were carried out with GAUSSIAN 88 and GAUSSIAN 90[14] with split valence (3-21G)[15] and polarization (6-31G*, 6-31G**)[16] basis sets. All geometries were fully optimized at the Hartree–Fock level with the 3-21G and 6-31G* basis sets using analytical gradient methods; some structures were also optimized at the MP2/6-31G* or MP2/6-31G** levels. Vibrational frequencies and zero point energies were obtained at the HF/6-31G* level using analytical second derivatives. Fourth order Møller–Plesset perturbation theory in the space of single, double, triple, and quadruple excitations (MP4SDTQ, frozen core) was used to estimate electron correlation energy. For some transition states, the reaction path was followed in internal coordinates[17] (nonmass weighted, step size = 0.4 au or rad) to confirm the mechanism of the reaction.

Results and Discussion

The calculated total energies for the clusters and transition states for reactions 1–17 are given in Table I. The total energies for the reactants and products have been published previously.[3,4] The vibrational frequencies calculated at the HF/6-31G* level are listed in Table II, and the optimized geometries for the transition state and clusters are given in Figures 1–7. Table III presents the calculated barriers for the silylene insertion reactions; Table IV shows the cluster well-depths. The computed thermal decomposition barriers are collected in Table V.

Geometries. SiXY + H_2. The HF/3-21G, HF/6-31G*, and MP2/6-31G** optimized transition structures for $SiH_4 \rightarrow SiH_2 + H_2$ are shown in Figure 1a. The geometries are very similar and are characterized by a short SiH_2–H_2 distance with the H_2 in the symmetry plane. Replacing one or both of the silylene hydrogens with fluorine does not change the configuration very much (Figure 1b,c). With F substitution, the H–H, Si–H, and Si–H_2 bonds tend to lengthen and the angles open up. Beyond the transition state, SiXY + H_2 forms a weakly bound cluster

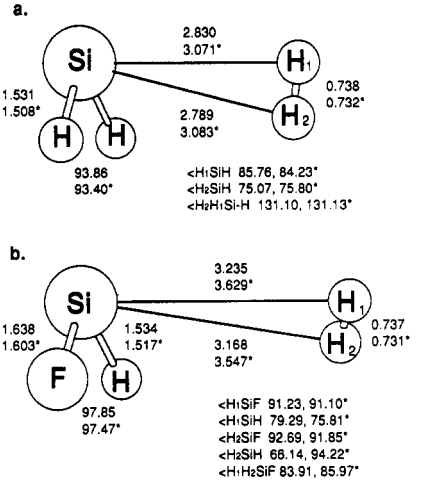

Figure 2. Clusters of SiH_2 and SiHF with H_2: no superscript, HF/3-21G optimized; asterisk, HF/6-31G* optimized.

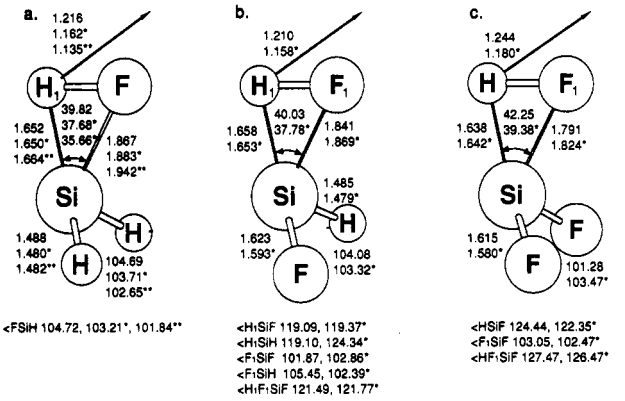

Figure 3. Transition structures for SiH_2, SiHF, and SiF_2 insertion into HF: no superscript, HF/3-21G optimized; asterisk, HF/6-31G* optimized; double asterisk, MP2/6-31G** optimized. Arrows indicate the HF/6-31G* transition vectors.

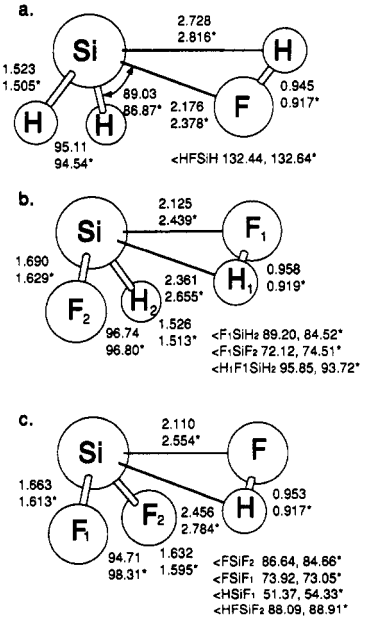

Figure 4. Clusters of SiH_2, SiHF, and SiF_2 with HF: no superscript, HF/3-21G optimized; asterisk, HF/6-31G* optimized.

(Figure 2), characterized by a very long Si–H_2 distance. The cluster is weakened by progressive F substitution to the extent that no stable cluster could be found for $SiF_2 + H_2$.[3]

SiXY + HF. The transition state for decomposition of SiHFXY into SiXY and HF (Figure 3a–c) is similar to that of $SiH_2XY \rightarrow SiXY + H_2$. The MP2-optimized transition state for SiH_2 +

(14) Frisch, M. J.; Head-Gordon, M.; Trucks, G. W.; Foresman, J. B.; Schlegel, H. B.; Raghavachari, K.; Robb, M.; Binkley, J. S.; Gonzalez, C.; DeFrees, D. J.; Fox, D. J.; Whiteside, R. A.; Seeger, R.; Melius, C. F.; Baker, J.; Martin, L. R.; Kahn, L. R.; Stewart, J. J. P.; Topiol, S.; Pople, J. A. *GAUSSIAN 90*; Gaussian, Inc.: Pittsburgh, PA, 1990.

(15) Binkley, J. S.; Pople, J. A.; Hehre, W. J. *J. Am. Chem. Soc.* **1980**, *102*, 939. Gordon, M. S.; Binkley, J. S.; Pople, J. A.; Pietro, W. J.; Hehre, W. J.; *J. Am. Chem. Soc.* **1982**, *104*, 2797.

(16) Hariharan, P. C.; Pople, J. A. *Theor. Chim. Acta* **1973**, *28*, 213 and references cited therein. Francl, M. M.; Pietro, W. J.; Hehre, W. J.; Binkley, J. S.; Gordon, M. S.; DeFrees, D. J.; Pople, J. A. *J. Chem. Phys.* **1982**, *77*, 3654 and references cited therein; the 6-31G(d) and 6-31G(d,p) basis sets are the same as those in 6-31G* and 6-31G**, respectively.

(17) Gonzalez, C.; Schlegel, H. B. *J. Chem. Phys.* **1989**, *90*, 2154.

TABLE I: Total Energies[a]

	6-31G*				6-31G**					6-31G*
	HF	E_2	E_3	E_{4SDQ}	HF	E_2	E_3	E_{4SDQ}	E_{4T}	ZPE
SiH_4	−291.225 13	−0.081 89	−0.018 38	−0.004 70	−291.230 84	−0.108 15	−0.021 00	−0.004 26	−0.001 35	21.02
$SiH_2 + H_2$ (cl)	−291.127 17	−0.085 10	−0.022 20	−0.006 42	−291.134 70	−0.107 78	−0.023 71	−0.005 97	−0.001 13	15.93
$SiH_2 + H_2$ (ts)	−291.097 65	−0.101 46	−0.022 03	−0.005 17	−291.108 67	−0.125 95	−0.023 07	−0.004 37	−0.002 81	18.13
$SiH_2 + H_2$	−291.126 61	−0.084 55	−0.022 21	−0.006 48	−291.133 96	−0.107 07	−0.023 69	−0.006 03	−0.001 09	14.58
$SiH_3 + H$	−291.104 36	−0.068 33	−0.016 05	−0.004 24	−291.108 82	−0.087 66	−0.017 82	−0.003 80	−0.001 16	14.35
SiH_3F	−390.148 40	−0.251 30	−0.010 83	−0.007 77	−390.152 84	−0.271 35	−0.013 04	−0.007 68	−0.004 69	18.61
$SiHF + H_2$ (cl)	−390.059 04	−0.259 70	−0.013 85	−0.010 49	−390.065 13	−0.275 75	−0.014 86	−0.010 27	−0.005 28	13.20
$SiHF + H_2$ (ts)	−389.996 93	−0.291 64	0.004 77	−0.009 02	−390.007 06	−0.289 50	−0.015 91	−0.008 59	−0.006 29	15.40
$SiHF + H_2$	−390.058 73	−0.259 49	−0.013 85	−0.010 52	−390.064 74	−0.275 44	−0.014 85	−0.010 28	−0.005 26	12.44
$SiH_2 + HF$ (cl)	−390.013 51	−0.251 60	−0.016 92	−0.007 88	−390.024 93	−0.269 13	−0.018 33	−0.007 65	−0.003 50	16.75
$SiH_2 + HF$ (ts)	−389.973 44	−0.277 48	−0.009 04	−0.010 47	−389.982 11	−0.294 99	−0.010 34	−0.010 43	−0.008 15	15.17
$SiH_2 + HF$	−390.002 69	−0.245 95	−0.018 87	−0.007 54	−390.014 18	−0.263 71	−0.020 03	−0.007 32	−0.003 38	14.17
$SiH_2F + H$	−390.021 07	−0.238 41	−0.008 11	−0.007 63	−390.024 14	−0.247 90	−0.013 00	−0.007 50	−0.004 69	11.99
$SiH_3 + F$	−389.971 08	−0.190 64	−0.024 47	−0.006 00	−389.975 54	−0.209 97	−0.026 24	−0.005 56	−0.002 36	14.35
SiH_2F_2	−489.081 81	−0.422 88	−0.003 57	−0.010 94	−489.084 83	−0.436 26	−0.005 14	−0.010 99	−0.008 26	15.70
$SiF_2 + H_2$ (ts)	−488.902 26	−0.443 04	−0.007 75	−0.013 10	−488.911 37	−0.454 41	−0.008 04	−0.012 84	−0.010 19	12.21
$SiF_2 + H_2$	−489.011 50	−0.436 06	−0.005 44	−0.014 12	−489.016 00	−0.445 11	−0.005 79	−0.013 94	−0.009 61	9.86
SiHF + HF (cl)	−488.947 63	−0.425 76	−0.009 61	−0.009 69	−488.957 63	−0.436 81	−0.010 11	−0.011 55	−0.008 02	14.28
SiHF + HF (ts)	−488.899 64	−0.450 48	−0.001 12	−0.014 10	−488.906 90	−0.461 43	−0.001 88	−0.014 25	−0.012 10	12.28
SiHF + HF	−488.934 81	−0.420 89	−0.010 51	−0.011 58	−488.944 96	−0.432 08	−0.011 19	−0.011 57	−0.007 55	12.03
$SiH_2 + F_2$ (cl)	−488.679 15	−0.422 60	−0.016 22	−0.012 25	−488.682 01	−0.436 11	−0.017 35	−0.011 98	−0.009 49	10.67
$SiH_2 + F_2$ (ts-syn)	−488.635 84	−0.502 09	0.004 55	−0.017 17	−488.638 86	−0.515 34	0.003 63	−0.016 24	−0.029 84	11.84
$SiH_2 + F_2$ (ts-anti)	488.659 92	−0.484 43	0.001 87	−0.017 16	−488.662 82	−0.497 83	0.000 75	−0.016 61	−0.023 76	11.69
$SiH_2 + F_2$	−488.677 54	−0.419 99	−0.016 90	−0.020 05	−488.680 39	−0.433 46	−0.018 03	−0.011 72	−0.009 15	9.72
$SiHF_2 + H$	−488.949 06	−0.410 30	−0.000 36	−0.011 03	−488.950 61	−0.416 73	−0.001 04	−0.011 01	−0.008 40	9.06
$SiH_2F + F$	−488.887 79	−0.360 72	−0.016 53	−0.009 39	−488.890 86	−0.370 21	−0.021 42	−0.009 26	−0.005 89	11.99
$SiHF_3$	−588.018 33	−0.594 58	0.003 17	−0.013 87	−588.019 85	−0.601 15	0.002 36	−0.013 93	−0.011 85	12.28
SiF_2 + HF (cl)	−587.898 38	−0.601 08	−0.001 42	−0.015 11	−587.906 90	−0.605 18	−0.001 45	−0.015 16	−0.012 20	10.98
SiF_2 + HF (ts)	−587.837 00	−0.624 76	−0.006 76	−0.017 41	−587.842 44	−0.628 89	0.006 68	−0.017 60	−0.016 21	8.90
SiF_2 + HF	−587.887 58	−0.597 46	−0.002 10	−0.015 18	−587.896 22	−0.601 75	−0.002 13	−0.015 23	−0.011 90	9.45
SiHF + F_2 (cl)	−587.610 96	−0.559 69	−0.008 08	−0.016 25	−587.612 47	−0.603 88	−0.008 73	−0.016 16	−0.013 57	8.42
SiHF + F_2 (ts-syn)	−587.555 68	−0.690 36	0.013 57	−0.018 83	−587.557 40	−0.696 88	0.013 31	−0.017 93	−0.037 44	8.58
SiHF + F_2 (ts-anti)	−587.585 54	−0.664 44	0.010 64	−0.020 61	−587.587 04	−0.671 19	0.010 04	−0.020 27	−0.029 64	8.66
SiHF + F_2	−587.609 66	−0.594 93	−0.008 54	−0.024 09	−587.611 17	−0.601 83	−0.009 19	−0.015 97	−0.013 32	7.58
$SiF_3 + H$	−587.879 47	−0.581 60	0.006 97	−0.014 01	−587.879 47	−0.581 60	0.006 97	−0.014 01	−0.012 06	5.76
$SiHF_2 + F$	−587.815 78	−0.532 61	−0.008 78	−0.012 79	−587.817 33	−0.539 04	−0.009 46	−0.012 77	−0.009 60	9.06
SiF_4	−686.949 84	−0.764 61	0.009 17	−0.016 37	−686.949 84	−0.764 61	0.009 17	−0.016 37	−0.015 35	8.49
$SiF_2 + F_2$ (cl)	−686.563 50	−0.773 29	0.000 24	−0.019 80	−686.563 50	−0.773 29	0.000 24	−0.019 80	−0.017 84	5.26
$SiF_2 + F_2$ (ts-anti)	686.522 22	−0.860 01	0.019 90	−0.019 29	−686.522 22	−0.860 01	0.019 90	−0.019 29	−0.038 50	5.42
$SiF_2 + F_2$	−686.562 43	−0.771 50	−0.000 13	−0.027 69	−686.562 43	−0.771 50	−0.000 13	−0.019 63	−0.017 67	5.00
$SiF_3 + F$	−686.746 19	−0.703 91	−0.001 45	−0.015 77	−686.746 19	−0.703 91	−0.001 45	−0.015 77	−0.013 26	5.76

[a] Total energies in atomic units; zero point energies in kcal/mol.

TABLE II: Frequencies[a]

molecule	frequencies
	Transition States
SiH_2--H_2	1630*i*, 837, 863, 1027, 1125, 1782, 2263, 2382, 2400
SiHF--H_2	1786*i*, 671, 762, 887, 923, 1146, 1635, 2312, 2436
SiF_2--H_2	1993*i*, 342, 612, 761, 926, 995, 1034, 1473, 2397
SiHF--HF	1860*i*, 227, 516, 714, 815, 939, 990, 2027, 2366
SiF_2--HF	1863*i*, 208, 279, 390, 661, 699, 957, 1007, 2028
SiH_2--HF	1886*i*, 497, 619, 778, 880, 1095, 2020, 2359, 2360
SiH_2--F_2 (syn)	1036*i*, 221, 256, 607, 733, 845, 1016, 2290, 2318
SiH_2--F_2 (anti)	748*i*, 185, 285, 579, 630, 813, 1089, 2294, 2304
SiHF--F_2 (syn)	963*i*, 126, 241, 303, 609, 719, 857, 939, 2210
SiHF--F_2 (anti)	729*i*, 111, 193, 289, 575, 749, 916, 954, 2276
SiF_2--F_2 (anti)	648*i*, 102, 103, 285, 325, 431, 593, 951, 1004
	Clusters
SiH_2--H_2	90, 95, 209, 236, 345, 1129, 2208, 2219, 4611
SiHF--H_2	31, 69, 79, 133, 234, 921, 964, 2169, 4632
SiH_2--F_2	46, 47, 73, 213, 285, 1131, 1241, 2210, 2220
SiHF--F_2	33, 62, 103, 105, 351, 919, 968, 1288, 2059
SiHF--HF	132, 194, 332, 504, 570, 867, 966, 2181, 4243
SiF_2--HF	88, 135, 179, 284, 374, 522, 894, 934, 4271
SiH_2--HF	157, 167, 419, 478, 646, 1120, 2220, 2230, 4283
SiF_2--F_2	7, 22, 40, 53, 55, 373, 932, 948, 1243

[a] In cm^{-1} at the HF/6-31G* level.

HF differs little from the Hartree–Fock-optimized geometry, suggesting the HF/6-31G* level is adequate for the fluorine-substituted cases. The Si–F distance in SiXY--HF decreases with F substitution while the Si–H distance remains the same. The transition vectors for insertion are dominated by the motion of

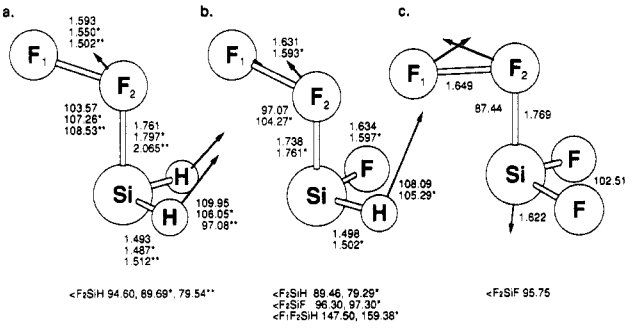

Figure 5. Transition structures for SiH_2, SiHF, and SiF_2 insertion into F_2 via the syn approach: no superscript, HF/3-21G optimized; asterisk, HF/6-31G* optimized. The MP2/6-31G*-optimized structure for $SiH_2 + F_2$ (double asterisk) is a second-order saddle point; all other structures are first-order saddle points.

the hydrogen and, hence, could be described equally well as a 1,2 hydrogen shift across the Si–F bond. The clusters (Figure 4a–c) are characterized by relatively short Si--F distances associated with the lone pair on the F interacting with the empty p_π orbital of silylene. With F substitution of the silylene, the Si–F distance in the cluster lengthens, suggesting a progressive weakening of the interaction. However, this is balanced by an interaction between the HF and SiF bond dipoles as indicated by the alignment of these bonds in SiHF--HF and SiF_2--HF.

SiXY + F_2. At the Hartree–Fock level, two families of transition structures can be found for silylene insertion into F_2: one

TABLE III: Barriers for Silylene-Insertion Reactions[a]

reactions	6-31G* HF	6-31G* MP2	6-31G* MP3	6-31G* MP4	6-31G** HF	6-31G** MP2	6-31G** MP3	6-31G** MP4[b]	6-31G** MP4[c]	HF/6-31G* ΔZPE
$SiH_2 + H_2 \rightarrow SiH_4$	21.7	11.1	11.2	12.0	19.4	7.6	8.0	9.0	7.9	3.5
$SiHF + H_2 \rightarrow SiH_3F$	41.7	21.6	33.3	34.2	39.2	30.3	29.7	30.7	30.1	3.0
$SiF_2 + H_2 \rightarrow SiH_2F_2$	70.9	66.5	65.1	65.7	68.0	62.2	60.8	61.5	61.1	2.3
$SiH_2 + HF \rightarrow SiH_3F$	19.4	−0.04	5.7	3.9	21.1	1.5	7.6	5.6	2.6	1.0
$SiHF + HF \rightarrow SiH_2F_2$	22.1	3.5	9.4	7.8	23.9	5.5	11.3	9.6	6.8	0.3
$SiF_2 + HF \rightarrow SiHF_3$	31.2	14.1	19.6	18.2	33.2	16.2	21.7	20.2	17.5	−0.6
$SiH_2 + F_2 \rightarrow SiH_2F_2$ (syn)	28.3	−23.2	−9.8	−8.0	28.2	−23.2	−9.6	−12.4	−25.4	2.1
(anti)	13.0	−27.4	−15.6	−13.8	13.0	−27.4	−15.6	−18.7	−27.8	2.0
$SiHF + F_2 \rightarrow SiHF_3$ (syn)	34.9	−25.0	−11.4	−13.0	34.7	−24.9	−10.7	−12.0	−27.3	1.0
(anti)	16.2	−27.4	−15.4	−13.2	16.2	−27.3	−15.2	−17.9	−28.2	1.1
$SiF_2 + F_2 \rightarrow SiF_4$ (anti)	25.7	−29.9	−17.3	−12.0	25.7	−29.9	−17.3	−17.1	−30.2	0.4

[a] ΔE in kcal/mol, with ΔZPE included, using the HF/6-31G*-optimized geometry. [b] Including single, double, and quadrupole excitations. [c] Including single, double, triple, and quadruple excitations.

TABLE IV: Cluster Well-Depths[a]

reaction	6-31G* HF	6-31G* MP2	6-31G* MP3	6-31G* MP4[b]	6-31G** HF	6-31G** MP2	6-31G** MP3	6-31G** MP4[b]	6-31G** MP4[c]	HF/6-316* ΔZPE
SiH_2--$H_2 \rightarrow SiH_2 + H_2$	0.4	0.7	0.7	0.6	0.5	0.9	0.9	0.9	0.9	−1.4
SiHF--$H_2 \rightarrow SiHF + H_2$	0.2	0.3	0.3	0.3	0.2	0.4	0.4	0.4	0.4	−0.8
SiH_2--$HF \rightarrow SiH_2 + HF$	6.8	10.3	9.1	9.3	6.8	10.2	9.0	9.2	9.2	−2.6
SiHF--$HF \rightarrow SiHF + HF$	8.1	11.1	10.4	7.5	8.0	10.9	10.2	10.2	10.5	−2.3
SiF_2--$HF \rightarrow SiF_2 + HF$	6.8	9.0	8.6	8.6	6.7	8.9	8.4	8.4	8.6	−1.5
SiH_2--$F_2 \rightarrow SiH_2 + F_2$	1.0	2.6	2.2	2.4	1.0	2.7	2.3	2.4	2.6	−1.0
SiHF--$F_2 \rightarrow SiHF + F_2$	3.6	0.8	2.1	1.8	0.8	2.1	1.8	1.9	2.1	−1.0
SiF_2--$F_2 \rightarrow SiF_2 + F_2$	0.7	1.8	1.5	1.6	0.7	1.8	1.5	1.6	1.8	−0.3

[a] ΔE in kcal/mol, with ΔZPE *not* included, using the HF/6-31G* optimized geometry. [b] Including single, double, and quadruple excitations. [c] Including single, double, triple and quadruple excitations.

with the migrating F syn to the silylene lone pair (Figure 5a–c) and the other with the F anti to the lone pair (Figure 6a–c). The latter is consistently lower in energy at the Hartree–Fock level. For both the syn and anti transition structures, the Si–F_2 bond is shorter than that in the corresponding SiXY + HF transition state. Fluorine substitution tends to shorten the Si–F bond and lengthen the F–Fbond. The syn transition state for $SiF_2 + F_2$ does not exist at the HF/6-31G* level; instead the optimization stepped monotonically to the anti conformer. Reaction path following[17] confirmed that the syn transition state proceeds to the fluorosilane product by the anticipated migration of the fluorine to the silylene lone pair. However, reaction path following showed that the anti transition structure reached the products by a backside attack on the lone pair with concomitant inversion of the silicon. Optimization of the syn transition state for $SiH_2 + F_2$ at the MP2/6-31G* level yields a structure that is significantly earlier on the reaction coordinate for insertion (Figure 5a). However, this structure is a second-order saddle point. The MP2 optimization and reaction path following for the anti approach revealed that insertion occurs without a barrier and proceeds to an intermediate that is ca. 80 kcal/mol more stable than the reactants (Figure 6a, similar in energy and structure to $SiH_2F + F$). This structure does not exist on the Hartree–Fock surface (optimization at the HF level starting from this structure leads directly to products). The unusual behavior of the HF and MP2 surfaces for $SiH_2 + F_2$ is, no doubt, related to the difficulty in treating the F_2 bond at simple levels of theory. Because SiXY + $F_2 \rightarrow SiXYF_2$ reactions are very exothermic (ca. 230–250 kcal/mol) and the F_2 bond is relatively weak (37 kcal/mol), these reactions may occur stepwise with F atom transfer to form SiXYF followed by radical recombination to form $SiXYF_2$. The possibility of a radicaloid mechanism is supported to some extent by the fact that the RHF-optimized transition state has a substantial UHF instability. The energy surface for $SiH_2 + F_2$ is being studied with higher levels of theory and larger basis sets.[18] Since the F_2-elimination

(18) Ayala, P. Y.; Ignacio, E. W.; Schlegel, H. B. Manuscript in preparation.

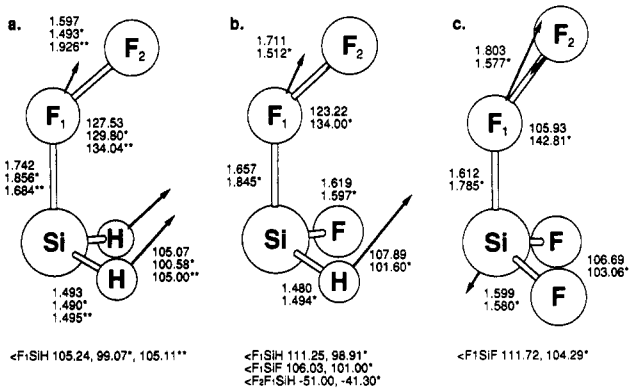

Figure 6. Transition structures for SiH_2, SiHF, and SiF_2 insertion into F_2 via the anti approach: no superscript, HF/3-21G optimized; asterisk, HF/6-31G* optimized. All structures are first-order saddle points except the MP2/6-31G*-optimized structure for $SiH_2 + F_2$ (double asterisk) which is a stable intermediate. On the MP2/6-31G* surface, the $SiH_2 + F_2$ reaction occurs without a barrier and proceeds to this low-energy intermediate.

channels for $SiH_{4-n}F_n$ lie 80–160 kcal/mol above the lowest energy pathways (see below), the uncertainties in the surfaces for SiXY + F_2 do not affect the mechanism for thermal decomposition.

The long-range clusters are shown in Figure 7a–c. The Si–F distances in SiXY + F_2 are longer than those in SiXY + HF and increase progressively with fluorine substitution, though not as much as the Si–H distances in SiXY + H_2.

Energetics. A previous study of the insertion of SiH_2, SiHF, and SiF_2 into H_2 found that there is a very large increase in the insertion barrier with fluorine substitution,[10] about 30 kcal/mol per fluorine as shown in Table III. For $SiH_2 + H_2$, the 7.9 kcal/mol barrier is reduced to 3.6 kcal/mol at the MP4/6-31+G(2df,p) level using the MP2/6-31G**-optimized geometry; more extensive calculations[1] lowered the barrier to 1.7 kcal/mol. The most recent analysis of the experimental data[12] yielded an activation energy of 0.5 kcal/mol; this suggest that the MP4/6-31G**

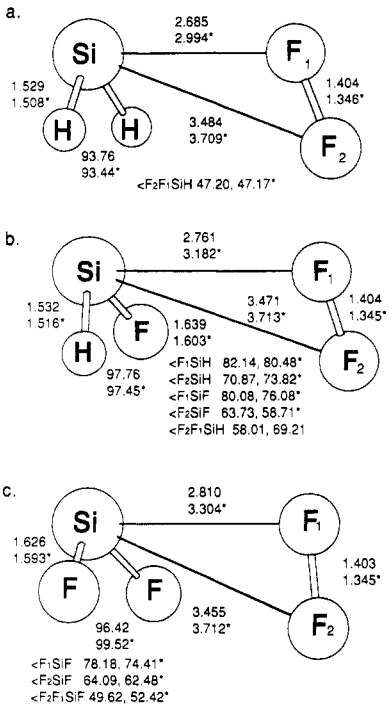

Figure 7. Clusters of SiH_2, SiHF, and SiF_2 with F_2: no superscript, HF/3-21G optimized; asterisk, HF/6-31G* optimized.

TABLE V: Thermal Decomposition Barriers of SiH_nF_{4-n}[a]

reaction	$\Delta H_r(0)$	forward barrier	reverse barrier
SiH_4			
→ $SiH_2 + H_2$	55	57	2
→ $SiH_3 + H$	89	89	0
SiH_3F			
→ $SiHF + H_2$	46	70	24
→ $SiH_2 + HF$	84	91	7
→ $SiH_2F + H$	92	92	0
→ $SiH_3 + F$	150	150	0
SiH_2F_2			
→ $SiF_2 + H_2$	31	86	55
→ $SiHF + HF$	82	93	11
→ $SiHF_2 + H$	94	94	0
→ $SiH_2F + F$	159	159	0
→ $SiH_2 + F_2$	250	≥250	≥0
$SiHF_3$			
→ $SiF_2 + HF$	68	89	21
→ $SiF_3 + H$	98	98	0
→ $SiHF_2 + F$	163	163	0
→ $SiHF + F_2$	249	≥249	≥0
SiF_4			
→ $SiF_3 + F$	163	163	0
→ $SiF_2 + F_2$	232	≥232	≥0

[a] In kcal/mol.

values are too high by ca. 6 kcal/mol. The SiXY + H_2 barriers listed in Table V are calculated using isodesmic reaction 21 at the MP4SDTQ/6-31G** level combined with the best available theoretical value for $SiH_2 + H_2 \rightarrow SiH_2$–$H_2$ (ts) (1.7 kcal/mol).

$$SiXY_2 + H_2 + SiH_2\text{–}H_2\ (ts) \rightarrow SiXY_2\text{–}H_2\ (ts) + SiH_2 + H_2\ (X, Y = H, F) \quad (21)$$

For SiH_2, SiHF, and SiF_2 insertion into HF, the barriers are small and the increase in barrier on F substitution on the silylene is much less than that for insertion into H_2, about 5–10 kcal/mol per F. For SiH_2 + HF, higher level calculations (MP4/6-31+G(2df,p)) using the MP2/6-31G**-optimized geometry give an insertion barrier of 6.6 kcal/mol. This suggests a systematic error of ca. +4 kcal/mol. Similar to the SiXY + H_2 insertion barriers, the barriers for insertion into HF listed in Table V have been computed using isodesmic reaction 22 at the MP4/6-31G** level

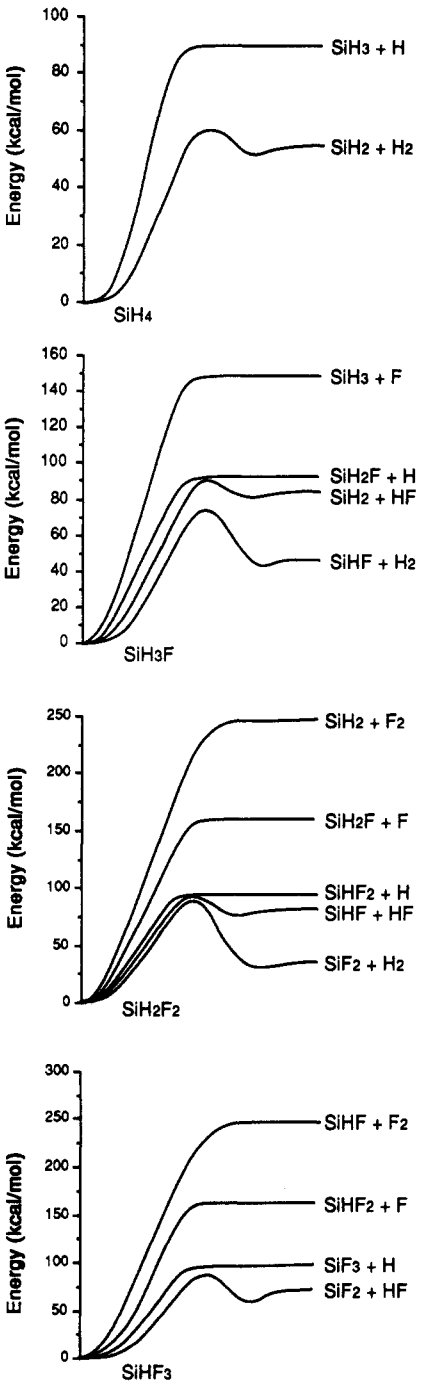

Figure 8. Potential energy profiles for the various channels for the thermal decomposition of SiH_4, SiH_3F, SiH_2F_2, and $SiHF_3$.

combined with a value of 6.6 kcal/mol for $SiH_2 + HF \rightarrow Si$-$H_2$–HF (ts) obtained from the higher level calculations.

$$SiXY_2 + HF + SiH_2\text{–}HF\ (ts) \rightarrow SiXY_2\text{–}HF\ (ts) + SiH_2 + HF\ (X, Y = H, F) \quad (22)$$

At the Hartree–Fock level, the barrier for SiXY insertion into F_2 is 15–20 kcal/mol lower for the anti transition state than for the syn. With fluorine substitution, the barrier increases by ca. 5 kcal/mol per fluorine. When correlation corrections are computed at the Hartree–Fock-optimized geometries, the barriers change drastically (dropping by 30–50 kcal/mol); this is due to the dramatic differences between the HF and MP2 potential energy surfaces and optimized geometries discussed above. The MP2/6-31G* optimizations and reaction path following indicate that there is no barrier for SiH_2 insertion into F_2. Even in the absence of a barrier for insertion, the SiXY + F_2 decomposition channel is disfavored by 80–160 kcal/mol compared to other pathways.

The cluster well-depths are listed in Table IV. The clusters between the silylenes and H_2 are weakly bound (<1 kcal/mol), and the binding energy decreases with fluorine substitution of the silylenes. The clusters with HF are more strongly bound (ca. 10 kcal/mol), reflecting the donation of the fluorine lone pair into the empty p_π orbital of the silylene as well as the dipole–dipole interaction. The well-depth for the clusters with F_2 are intermediate between those of H_2 and HF.

Figure 8a shows the thermal decomposition of SiH_4 to $SiH_2 + H_2$ as the preferred path with a barrier of ca. 57 kcal/mol. The $SiH_3 + H$ channel is higher by about 30 kcal/mol. Figure 8b shows the four lowest energy pathways for the SiH_3F decomposition. The $SiHF + H_2$ channel is the favored, with a barrier of 70 kcal/mol; the $SiH_2 + HF$ and $SiH_2F + H$ paths lie ca. 20 kcal/mol higher, with barriers of 91 and 92 kcal/mol, respectively. The $SiH_3 + F$ channel is 150 kcal/mol above that of SiH_3F. For the decomposition of SiH_2F_2 (Figure 8c), there are three closely competing channels, $SiF_2 + H_2$, $SiHF + HF$, and $SiHF_2 + H$, each with barriers of ca. 90 kcal/mol. The other two channels, $SiH_2F + F$ and $SiH_2 + F_2$, are very much higher in energy, with barriers 159 and ≥250 kcal/mol, respectively. Elimination of HF is the preferred pathway for $SiHF_3$, with Si–H bond cleavage being 9 kcal/mol higher (Figure 8d). For SiF_4 decomposition, breaking a single SiF is overwhelmingly favored over F_2 elimination.

The thermal decompositions of SiH_4, SiH_3F, and SiH_2F_2 diluted in Ar have been studied by shock tube methods.[9] The temperature and pressure dependences of the reaction rates have been fitted using Troe's approach. The threshold obtained for SiH_4 (59 kcal/mol) agrees well with the calculated barrier (57 kcal/mol[1]). The E_0 for SiH_3F decomposition (62 kcal/mol) is consistent with the heat of reaction for the $SiHF + H_2$ channel (ΔH_r = 46 kcal/mol) but not for the $SiH_2 + HF$ channel (ΔH_r = 84 kcal/mol). However, the E_0 from the fit of the experimental data (62 kcal/mol) is lower than the calculated barrier (70 kcal/mol), suggesting the latter is overestimated by 8 kcal/mol. For SiH_2F_2, the fitting yields E_0 = 72 kcal/mol, ruling out the $SiHF + HF$ and $SiHF_2 + H$ channels (ΔH_r = 84 and 94 kcal/mol, respectively) and suggests the theoretical barrier for $SiH_2F_2 \rightarrow SiF_2 + H_2$ (86 kcal/mol) is overestimated by 14 kcal/mol. However, because the experimental data is far from the high-pressure limit and spans a narrow range of pressures, some caution is required in interpreting the results.

Acknowledgment. We wish to thank the Wayne State University Computing Services and the Pittsburgh Supercomputer Center for generous allocations of computer time. This work was supported by a grant from the National Science Foundation (CHE 90-20398).

Registry No. SiH_4, 7803-62-5; SiH_3F, 13537-33-2; SiH_2F_2, 13824-36-7; $SiHF_3$, 13465-71-9; SiF_4, 7783-61-1.

Spin Potential in Kohn–Sham Theory

Marcelo Galván*,† and Rubicelia Vargas

Departamento de Química, División de Ciencias Básicas e Ingeniería, Universidad Autónoma Metropolitana-Iztapalapa, A.P. 55-534, México, D.F. 09340, Mexico *(Received: July 8, 1991)*

The spin potential, a recently defined quantity (Galván, M.; Vela, A.; Gázquez, J. L. *J. Phys. Chem.* **1988**, *92*, 6470), is obtained for atoms from $Z = 3$ to $Z = 54$ within the framework of spin-polarized Kohn–Sham theory in the local density approximation. It is shown that this quantity has periodic behavior such as the electronegativity or ionization potential. A relationship between spin potential and processes in which the system changes its multiplicity at a constant number of electrons is established. This relationship is used to calculate pairing energies. Then, spin potential emerges as a measure of the tendency of a system to change its spin polarization.

Introduction

One of the most encouraging features of density functional theory (DFT)[1] is that it has given a framework to rationalize such concepts as electronegativity[2] and hardness and softness,[3] and it has also motivated the definition of new quantities that have been proven to be useful as reactivity criteria (i.e., the Fukui function[4] and local softness and local hardness[5]).

On the other hand, it is well-known that the spin-polarized version of DFT improves the description of electronic structure of atoms, molecules, and solids.[6] Besides quantities such as electronegativity, hardness, and the Fukui function, some new global and local parameters appear in this theory: the generalized Fukui functions and hardnesses and the spin potential.[7] Within this theory, the energy functional in the absence of a magnetic field is expressed in the form[8,9]

$$E[\rho,\rho_s,\vartheta(\mathbf{r})] = F[\rho,\rho_s] + \int \vartheta(\mathbf{r})\,\rho(\mathbf{r})\,d\mathbf{r} \qquad (1)$$

where $\rho(\mathbf{r}) = \rho_\uparrow(\mathbf{r}) + \rho_\downarrow(\mathbf{r})$ is the total charge density, $\rho_s(\mathbf{r}) = \rho_\uparrow(\mathbf{r}) - \rho_\downarrow(\mathbf{r})$ is the spin density, and $\vartheta(\mathbf{r})$ is the external potential. In this formalism, the charge and spin distributions are independent variables; thus there are two Euler equations associated with the energy-minimization process:[7]

$$\mu_N = \left(\frac{\delta E}{\delta \rho(\mathbf{r})}\right)_{\rho_s,\vartheta(\mathbf{r})} = \vartheta(\mathbf{r}) + \frac{\delta F}{\delta \rho(\mathbf{r})} \qquad (2)$$

$$\mu_s = \left(\frac{\delta E}{\delta \rho_s(\mathbf{r})}\right)_{\rho,\vartheta(\mathbf{r})} = \frac{\delta F}{\delta \rho_s(\mathbf{r})} \qquad (3)$$

μ_N and μ_s are, respectively, the Lagrange multipliers associated with the restrictions

$$\int \rho(\mathbf{r})\,d\mathbf{r} = N = N_\uparrow + N_\downarrow \qquad (4)$$

$$\int \rho_s(\mathbf{r})\,d\mathbf{r} = N_s = N_\uparrow - N_\downarrow \qquad (5)$$

† Present address: Department of Physics, Massachusetts Institute of Technology, Cambridge, MA 02139.

(1) Parr, R. G.; Yang, W. *Density Functional Theory of Atoms and Molecules*; Oxford University Press: New York, 1989.
(2) Parr, R. G.; Donnelly, R. A.; Levy, M.; Palke, W. E. *J. Chem. Phys.* **1978**, *68*, 3801.
(3) Parr, R. G.; Pearson, R. G. *J. Am. Chem. Soc.* **1983**, *105*, 7512.
(4) Parr, R. G.; Yang, W. *J. Am. Chem. Soc.* **1984**, *106*, 4049.
(5) Berkowitz, M.; Parr, R. G. *J. Chem. Phys.* **1988**, *88*, 2554.
(6) Slater, J. C. *Quantum Theory of Molecules and Solids*; McGraw-Hill: New York, 1974; Vol. 4.
(7) Galván, M.; Vela, A.; Gázquez, J. L. *J. Phys. Chem.* **1988**, *92*, 6470.
(8) von Barth, U.; Hedin, L. *J. Phys. C* **1972**, *5*, 1629.
(9) Vosko, S. H.; Perdew, J. P. *Can. J. Phys.* **1975**, *53*, 1385.

0022-3654/92/2096-1625$03.00/0